Journal of Molecular Structure 1321 (2025) 139778

Contents lists available at ScienceDirect

Journal of Molecular Structure

journal homepage: www.elsevier.com/locate/molstr

Glucoimines incorporating classical and non-classical carbonic anhydrase pharmacophores: Design, synthesis, conformational analysis, biological evaluation, and docking simulations

Ivana R. Vásquez [a,1], Leonardo E. Riafrecha [1,a], Leandro Martínez Heredia [c], Gustavo A. Echeverría [b], Oscar E. Piro [b], Martín J. Lavecchia [c], Claudiu T. Supuran [d], Pedro A. Colinas [a,*]

[a] CEDECOR (UNLP-CICBA), CONICET, Departamento de Química, Facultad de Ciencias Exactas, Universidad Nacional de La Plata, 47 y 115, 1900 La Plata, Argentina
[b] Departamento de Física, Facultad de Ciencias Exactas, Universidad Nacional de La Plata and Institute IFLP (CONICET, CCT-La Plata), C. C. 67, 1900 La Plata, Argentina
[c] CEQUINOR (UNLP-CONICET, CCT-La Plata, associated with CIC), Departamento de Química, Facultad de Ciencias Exactas, Universidad Nacional de La Plata Blvd. 120 1465, La Plata, Argentina
[d] Università degli Studi di Firenze, NEUROFARBA Department, Section of Pharmaceutical Chemistry, Via Ugo Schiff 6, 50019 Sesto Fiorentino (Florence), Italy

ARTICLE INFO

Keywords:
Imines
Cancer
Enzyme inhibitor

ABSTRACT

In this report, a series of glucoimines has been prepared by reaction of d-glucosamine and aromatic aldehydes incorporating classical and non-classical carbonic anhydrase pharmacophores. The conformational behavior of veratrole glucoimine was studied in solution and in crystalline form, by NMR and X-ray diffraction analysis, which revealed that pyranose ring adopted a $^4C_1$ conformation. All glucoimines were tested against four isozymes of carbonic anhydrase: hCAs I and II (cytosolic, ubiquitous isozymes) and hCAs IX and XII (tumor-associated isozymes). In this study, per-O-acetylated and deprotected sulfonamide were identified as potent inhibitors of tumor-associated carbonic anhydrase isoforms. Molecular docking simulation was performed inside the active site of hCA II to evaluate the binding modes of veratrole and sulfonamide glucoimines. The last ones demonstrated the most favorable docking scores, indicating strong binding affinity towards hCAII in correlation with experimental inhibition activities. Interestingly, interaction analyses revealed distinct binding modes for ligand-hCAII complexes primarily due to the sulfonamide group.

1. Introduction

Imines or Schiff bases, compounds first described by Hugo Schiff, are easily prepared by condensation of carbonyl derivatives and primary amines [1]. The mechanism involves the nucleophilic addition of the amine to the carbonyl group with the formation of a carbinolamine, which suffers dehydration to generate the imine [2]. In sugar chemistry, a large number of Schiff bases has been described by reaction of 2-amino carbohydrates with aldehydes. The first example of these sugar imines was described in 1913 [3], and since then, several have been employed in stereoselective synthesis and as protective groups [4]. Also, glycoimines and their complexes have shown biological activities such as glucosidase inhibitors and antiproliferative agents [5-9].

Since several years ago our group has been interested in the design of glyco-inhibitors of carbonic anhydrase (CA) isozymes [10,11]. CAs catalyze one of the most important physiological reactions: the reversible hydration of carbon dioxide with the formation of proton and bicarbonate [12]. Among the 15 different α-CA isoforms known in humans, two isozymes, hCAs XI and XII, are upregulated in many hypoxic tumors and contribute to the acidic extracellular pH of the tumor microenvironment [13]. Consequently, one anticancer therapy has focused on the inhibition of these transmembrane isoforms. Our group has developed several inhibitors of the tumor-associated CA isozymes by attachment of carbohydrate moieties to CA pharmacophores [11,14]. In this report we described the synthesis of glucoimines incorporating classical (sulfonamide) and non-classical (methoxyaryl and phenol) CA

* Corresponding author.
E-mail address: pcolinas@quimica.unlp.edu.ar (P.A. Colinas).
[1] Both authors contributed equally to this report

https://doi.org/10.1016/j.molstruc.2024.139778
Received 20 May 2024; Received in revised form 21 August 2024; Accepted 22 August 2024
Available online 28 August 2024
0022-2860/© 2024 Elsevier B.V. All rights are reserved, including those for text and data mining, AI training, and similar technologies.

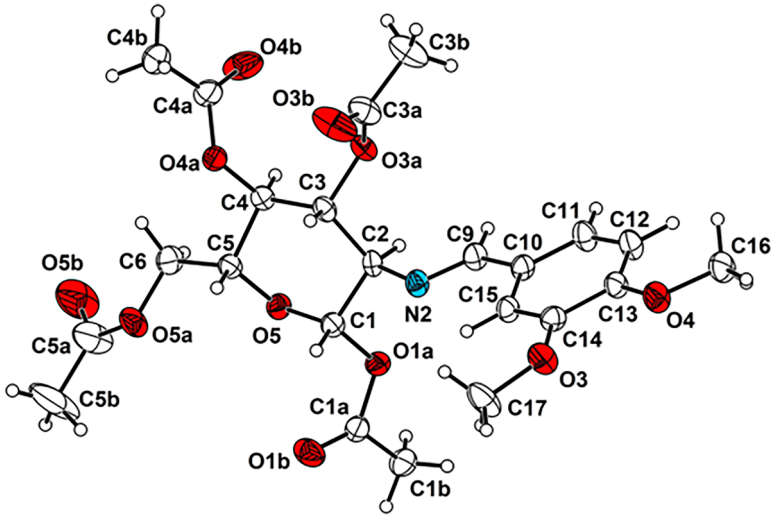

Fig. 1. View of glucoimine **5ii**, showing the labeling of the non-H atoms and their displacement ellipsoids at the 30 % probability level.

pharmacophores and screened them as CA inhibitors (Fig. 1). We also studied their conformational behavior in solution and crystalline form and molecular docking study has been performed to shed light on the binding modes in the CA active site.

2. Experimental

2.1. Chemistry

2.1.1. General procedure 1: preparation of glucoimines *2* and *6i-iv*

Commercially available d-glucosamine hydrochloride **1** (640 mg, 3 mmol), was poured in a solution of $NaHCO_3$ (330 mg, 3.9 mmol) and 2.60 mL of water at room temperature. After 5 min and complete dissolution, substituted benzaldehyde (3.4 mmol) dissolved in 2.30 mL of methanol was poured into the reaction mixture. It was stirred at room temperature for 1 hour and then left for 3 h at 0 °C. The precipitate was filtered, rinsed with cold water and 1:1 methanol/ether, and dried *in vacuo*. The crude material (**2, 6ii,** and **6ii**) was crystallized from ethanol, and (**6i**) from H_2O/EtOH.

N-[methoxybenzylidene]-d-glucosamine (**2**) Yield: 77 %. White solid. mp = 154–156 °C. ^{1}H NMR (300 MHz, DMSO-d6): δ 2.76–2.81 (m, 1H, CH), 3.10–3.17 (m, 1H, CH), 3.20–3.25 (m, 1H, CH), 3.40–3.52 (m, 2H, CH2), 3.70–3.75 (m, 1H, CH), 3.80 (s, 3H, OCH3), 4.54 (t, *J* = 6.0 Hz, 1H, OH), 4.69 (d, *J* = 7.3 Hz, 1H, OH), 4.80 (d, *J* = 5.7 Hz, 1H, OH), 4.91 (d, *J* = 5.0 Hz, 1H, OH), 6.51 (s, 1H, CH), 6.96–7.01 (m, 2H, 2 × ArCH), 7.66–7.72 (m, 2H, 2 × ArCH), 8.11 (s, 1H, CH); ^{13}C NMR (75 MHz, DMSO-d6): δ 55.7 (O CH_3), 61.7 (CH2), 70.8 (CH), 75.1 (CH), 77.3 (CH), 78.7 (CH), 96.1 (CH), 114.4 (2 × ArCH), 129.6 (ArC), 130.1 (2 × ArCH), 161.5 (C), 161.7 (C).

N-[3-methoxy-4-hydroxybenzylidene]-d-glucosamine (**6i**) Yield: 54 %. Yellow solid. mp=166–166.5 °C. ^{1H} NMR (500 MHz, DMSO-d6) δ 9.75 (s, 1H, OH), 8.04 (s, 1H, CH), 7.33 (d, 1H, *J* = 1.8 Hz, ArH), 7.12 (dd, 1H, *J* = 8.1, 1.9 Hz, ArH), 6.82 (d, 1H, *J* = 8.0 Hz, ArH), 6.51 (d, 1H, *J* = 6.0 Hz, OH), 4.91 (m, 1H, OH), 4.78 (s, 1H, OH), 4.70 (dd, 1H, *J* = 8.1, 4.6 Hz, H-1), 4.54 (s, 1H, OH), 3.80 (s, 3H, CH_3O), 3.73 (m, 1H, H-6a), 3.49 (dd, 1H, *J* = 11.5, 5.9 Hz, H-6b), 3.43 (td, 1H, *J* = 9.1, 8.0, 4.8 Hz, H-4), 3.24 (ddd, 1H, *J* = 9.8, 5.9, 2.1 Hz, H-5), 3.14 (t, 1H, *J* = 9.2 Hz, H-3), 2.78 (dd, 1H, *J* = 9.3, 7.7 Hz, H-2).13C NMR (126 MHz, DMSO-d6) δ 162.14 (C-7), 149.53 (ArC), 148.23 (ArC), 128.51 (ArC), 123.23 (ArC), 115.57 (ArC), 110.54 (ArC), 96.09 (C-1), 78.68 (C-2), 77.27 (C-5), 75.08 (C-4), 70.88 (C-3), 61.75 (C-6), 55.98 (CH_3O).

N-[3,4-dimethoxybenzylidene]-d-glucosamine (**6ii**) Yield: 70 %. Pale solid. mp = 140-142 °C. 1H NMR (500 MHz, DMSO-d6) δ 8.10 (s, 1H, CH), 7.38 (dd, 1H, *J* = 21.7, 1.9 Hz, ArH), 7.24 (dd, 1H, *J* = 8.3, 1.9 Hz, ArH), 7.01 (d, 1H, *J* = 8.3 Hz, ArH), 6.53 (s, 1H, OH), 4.94 (m, 1H, OH), 4.83 (s, 1H, OH), 4.72 (d, 1H, *J* = 7.7 Hz, H-1), 4.55 (s, 1H, OH), 3.80 (s, 3H, CH_3O), 3.79 (s, 3H, CH_3O), 3.75 (d, 1H, *J* = 2.8 Hz, H-6a), 3.49 (m, 1H, H-6b), 3.44 (d, 1H, *J* = 9.1 Hz, H-4), 3.24 (m, 1H, H-5), 3.16 (m, 1H, H-3), 2.80 (dd, 1H, *J* = 9.3, 7.7 Hz, H-2).^{13}C NMR (126 MHz, DMSO-d6) δ 162.02 (C-7), 151.36 (ArC), 149.28 (ArC), 129.70 (ArC), 123.13 (ArC), 111.56 (ArC), 109.64 (ArC), 96.05 (C-1), 78.70 (C-2), 77.29 (C-5), 75.03 (C-4), 70.86 (C-3), 61.73 (C-6), 56.00 (CH_3O), 55.87 (CH_3O).

N-[4-sulfonamidebenzylidene]-d-glucosamine (**6iv**) Yield: 76 %. Yellow solid. Decomposition 150 °C. ^{1}H NMR (500 MHz, DMSO-d6) δ 8.28 (s, 1H, CH), 7.94 (m, 2H, 2 x ArH), 7.89 (m, 2H, 2 x ArH), 7.43 (s, 2H, NH_2), 4.96 (m, 1H, OH), 4.76 (d, 1H, *J* = 7.7 Hz, H-1), 3.74 (dd, 1H, *J* = 11.7, 2.1 Hz, OH), 3.48 (m, 3H, H-6a,H-6b,H-4), 3.35 (s, 2H, 2 x OH), 3.27 (ddd, 1H,*J* = 9.8, 5.9, 2.1 Hz, H-5), 3.18 (t, 1H, *J* = 9.1 Hz, H-3), 2.90 (dd, 1H, *J* = 9.3, 7.7 Hz, H-2).^{13}C NMR (126 MHz, DMSO-d6) δ 161.39 (C-7), 146.01 (ArC), 139.38 (ArC), 129.54 (ArC), 128.85 (ArC), 128.08 (ArC), 126.40 (ArC), 95.90 (C-1), 78.74 (C-2), 77.39 (C-5), 74.77 (C-4), 70.68 (C-3), 61.66 (C-6).

2.1.2 *(1,3,4,6)-Tetra-O-acetil-N-(4-methoxybenzylidene)-d-glucosamine* (**3**) Portionwise of dry *N*-[4-methoxybenzylidene]-d-glucosamine (1 g, 3.36 mmol) (**2**) was poured in a mixture of 6.40 mL of anhydrous pyridine and 3.20 mL of acetic anhydride cooled in an ice bath under continuous stirring. The reaction was kept stirring at 0 °C for 2 h. The cooling bath was removed, and the mixture was stirred at room temperature for an additional 48 h. Then, the yellowish solution was diluted with a large amount of water. The white precipitate was filtered off, washed with cold water, and dried *in vacuo*. The crude material was crystallized from ethanol.

Yield: 74 %. White solid. Mp: 178 °C- 179 °C. 1H NMR (500 MHz, DMSO-d6) δ 8.29 (s, 1H, CH), 7.66 (m, 2H, 2 x ArH), 7.00 (m, 2H, 2 x ArH), 6.08 (d, 1H, *J* = 8.2 Hz, H-1), 5.45 (t, 1H, *J* = 9.7 Hz, H-3), 4.98 (t, 1H, *J* = 9.7 Hz, H-4), 4.27 (ddd, 1H, *J* = 9.8, 4.7, 2.1 Hz, H-5), 4.23 (dd, 1H *J* = 12.2, 4.6 Hz, H-6a), 4.02 (dd, 1H,*J* = 12.3, 2.1 Hz, H-6b), 3.80 (s, 3H, CH_3O), 3.45 (dd, 1H, *J* = 9.8, 8.2 Hz, H-2), 2.03 (s, 3H, CH_3COO), 1.99 (d, 6H, *J* = 1.2 Hz, 2 x CH_3COO), 1.83 (s, 3H, CH_3COO).^{13}C NMR (126 MHz, DMSO-d6) δ 170.49 (CH_3COO), 169.89 (CH_3COO), 169.44 (CH_3COO), 169.05 (CH_3COO), 164.91 (C-7), 162.29 (ArC), 130.38 (2 x ArC), 128.73 (ArC), 114.66 (2 x ArC), 92.99 (C-1), 72.80 (C-2), 72.70 (C-3), 71.99 (C-5), 68.28 (C-4), 62.12 (C-6), 55.83 (CH_3O), 20.99 (CH_3CO), 20.91 (CH_3CO),20.91 (CH_3CO),20.65 (CH_3CO).

2.1.3. 1,3,4,6-Tetra-O-acetyl-β-D-glucosamine *(4)*

(1,3,4,6)-Tetra-*O*-Acetyl-*N*-(4-methoxybenzylidene)-glucosamine (1.53 g, 3.28 mmol) (**3**) was dissolved in 14 mL of acetone, then 0.78 mL

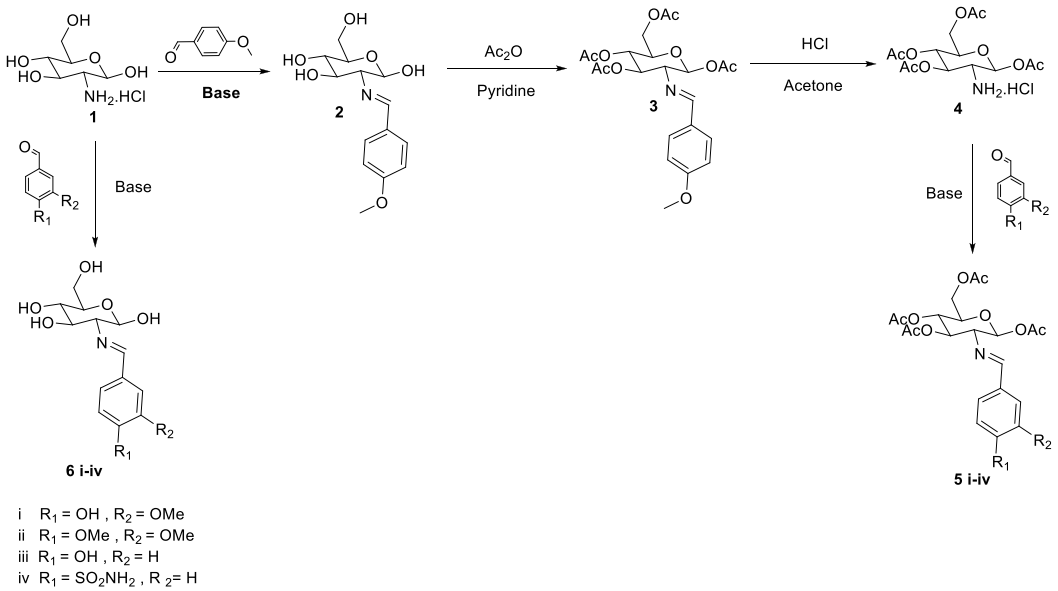

Scheme 1. Synthesis of per-O-acetylated and deprotected glucoimines.

Table 1
Selected torsion angles (in degrees) of glucoimine **5ii** and ideal $^4C_1$ pyranose ring.

Torsion angle	5ii	$^4C_1$[30]
O5-C1-C2-C3	48.4	60
C1-C2-C3-C4	−43.8	−60
C2-C3-C4-C5	49.6	60
C3-C4-C5-O5	−59.3	−60
C1-O5-C5-C4	68.5	60
C5-O5-C1-C2	−63.6	−60

of hydrochloric acid 5 M was added. The mixture was cooled in an ice-water bath for a few minutes and 14 mL of ethyl ether was added and stirring was kept for 2 h. The white precipitate was filtered and washed with cold ethyl ether. The solid is dried at 60 °C *in vacuo*. The product **4** was crystallized from methanol. Yield: 90 %

*2.1.4. General procedure 2: per-o-acetylated glucoimines (**5i-iv**)*

1,3,4,6-Tetra-O-acetyl-β-d-glucosamine (384 mg, 1 mmol) (**4**), was poured into a solution of $NaHCO_3$ (107 mg, 1.27 mmol) and 3.90 mL of water at room temperature. After 5 min, substituted benzaldehyde (1 mmol) dissolved in 0.80 mL MeOH was poured in the reaction mixture. It was stirred at room temperature for 3 h. The formed precipitate was filtered, rinsed with cold acetone, and dried under *in vacuo*. The crude material (**5i,5iii,** and **5iv**) was purified by chromatographic column (1:1 hexane:ethyl acetate), or (**6ii**) was crystallized from ethanol.

(1,3,4,6)-Tetra-O-Acetyl-N-(3-Methoxy-4-hydroxybenzylidene]-Glucosamine (**5i**) Yield: 36 %. Sticky colorless solid. ^{1}H NMR (500 MHz, DMSO-d6) δ 8.71 (s, 1H, OH), 8.63 (s, 1H, CH), 7.84 (d, 1 h J = 1.8 Hz, ArH), 7.68 (dd, 1H, J = 8.1, 1.8 Hz, ArH), 7.34 (d, 1H, J = 8.1 Hz, ArH), 6.48 (d, 1H, J = 8.3 Hz, H-1), 5.91 (t, 1H, J = 9.6 Hz, H-3), 5.54 (t, 1H, J = 9.8 Hz, H-4), 4.79 (dd, 1H, J = 12.3, 4.6 Hz, H-5), 4.64 (ddd, 1H, J = 10.0, 4.6, 2.3 Hz, H-6a), 4.57 (m, 1H, H-6b), 4.32 (s, 3H, CH_3O), 3.90 (dd, 1H, J = 9.8, 8.2 Hz, H-2), 2.49 (s, 3H, CH_3COO), 2.46 (s, 3H, CH_3COO), 2.45 (s, 3H, CH_3COO), 2.30 (s, 3H, CH_3COO).^{13}C NMR (126 MHz, DMSO-d6) δ 170.25 (CH_3COO), 169.77 (CH_3COO), 169.28 (CH_3COO), 168.79 (CH_3COO), 165.09 (C-7), 150.43 (ArC), 148.20 (ArC), 128.69 (ArC), 123.98 (ArC), 115.26 (ArC), 110.37 (ArC), 93.51 (C-1), 73.38 (C-2), 73.38 (C-3), 72.90 (C-5), 68.71 (C-4), 62.30 (C-6), 55.76 (CH_3O), 20.24 (CH_3CO), 20.22 (CH_3CO), 20.19 (CH_3CO), 20.07 (CH_3CO).

1.1.4.2 (1,3,4,6)-Tetra-O-Acetyl-N-(3,4-dimethoxybenzylidene]-Glucosamine (**5ii**). Yield: 48 %. White solid. Mp=174.5–175.5 °C. ^{1}H NMR (500 MHz, DMSO-d6) δ 8.26 (s, 1H, CH), 7.27 (m, 2H, 2 x ArH), 7.03 (d, 1H, J = 8.8 Hz, ArH), 6.10 (d, 1H, J = 8.3 Hz, H-1), 5.48 (t, 1H, J = 9.7 Hz, H-3), 4.98 (t, 1H, J = 9.7 Hz, H-4), 4.28 (ddd, 1H,J = 9.7, 4.6, 2.1 Hz, H-5), 4.23 (dd, 1H, J = 12.3, 4.6 Hz, H-6a), 4.02 (dd, 1H,J = 12.3, 2.1 Hz, H-6b), 3.80 (s, 3H, CH3O), 3.76 (s, 3H, CH_3O), 3.45 (dd, 1H, J = 9.7, 8.3 Hz, H-2), 2.03 (s, 3H, $CH_3$3COO), 2.00 (s, 3H, CH_3COO), 1.99 (s, 3H, CH_3COO), 1.83 (s, 3H, CH_3COO).^{13}C NMR (126 MHz, DMSO-d6) δ 170.50 (CH_3COO), 169.91 (CH_3COO), 169.46 (CH_3COO), 169.07 (CH_3COO), 165.16 (C-7), 152.16 (ArC), 149.38 (ArC), 128.85 (ArC), 123.39 (ArC), 111.82 (ArC), 109.95 (ArC), 92.97 (C-1), 72.81 (C-2), 72.78 (C-3), 71.95 (C-5), 68.30 (C-4), 62.12 (C-6), 56.09 (CH_3O), 55.91 (CH_3O), 21.00 (CH_3CO), 20.95 (CH_3CO), 20.91 (CH_3CO), 20.68 (CH_3CO).

(1,3,4,6)-Tetra-O-Acetyl-N-(4-hydroxybenzylidene]-Glucosamine (**5iii**) Yield: 30 %. White solid. Mp=176–178 °C. ^{1}H NMR (500 MHz, DMSO-d6) δ 9.36 (s, 1H, OH), 8.72 (s, 1H, CH), 8.08 (m, 2H, 2 x ArH), 7.34 (m, 2H, 2 x ArH), 6.47 (d, 1H, J = 8.3 Hz, H-1), 5.90 (t, 1H, J = 9.6 Hz, H-3), 5.54 (t, 1H, J = 9.8 Hz, H-4), 4.78 (dd, 1H, J = 12.2, 4.6 Hz, H-5), 4.63 (ddd, 1H, J = 10.1, 4.7, 2.2 Hz, H-6a), 4.57 (dd, 1H, J = 12.3, 2.3 Hz, H-6b), 3.89 (dd, 1H, J = 9.8, 8.3 Hz, H-2), 2.49 (s, 3H, CH_3COO), 2.46 (s, 3H, CH_3COO), 2.45 (s, 3H, CH_3COO), 2.30 (s, 3H, CH_3COO).^{13}C NMR (126 MHz, DMSO-d6) δ 170.25 (CH_3COO), 169.77 (CH_3COO), 169.24 (CH_3COO), 168.76 (CH_3COO), 164.86 (C-7), 160.87 (2 x ArC), 130.71 (ArC), 128.33 (ArC), 115.90 (2 x ArC), 93.51 (C-1), 73.39 (C-2), 73.37 (C-3), 72.91 (C-5), 68.70 (C-4), 62.29 (C-6), 20.23 (CH_3CO), 20.19 (CH_3CO), 20.19 (CH_3CO), 20.04 (CH_3CO).

(1,3,4,6)-Tetra-O-Acetyl-N-(4-sulfonamidebenzylidene]-Glucosamine (**5iv**) Yield: 30 %. Sticky colorless solid. ^{1}H NMR (500 MHz, DMSO-d6) δ 8.97 (s, 1H, CH), 8.41 (m, 4H, 4 x ArH), 7.15 (s, 2H, NH2), 6.55 (d, 1H, J = 8.2 Hz, H-1), 5.97 (t, 1H, J = 9.6 Hz, H-3), 5.57 (t, 1H, J = 9.8 Hz, H-4), 4.79 (dd, 1H, J = 12.3, 4.7 Hz, H-5), 4.68 (ddd, 1H, J = 10.0, 4.7, 2.3 Hz, H-6a), 4.58 (dd, 1H, J = 12.3, 2.3 Hz, H-6b), 4.04 (dd, 1H,J = 9.8, 8.2 Hz, H-2), 2.49 (s, 3H, CH_3COO), 2.47 (s, 3H, CH_3COO), 2.45 (s, 3H, CH_3COO), 2.31 (s, 3H, CH_3COO).^{13}C NMR (126 MHz, DMSO-d6) δ 170.24 (CH_3COO), 169.76 (CH_3COO), 169.28 (CH_3COO), 168.72 (CH_3COO), 164.52 (C-7), 146.93 (ArC), 139.18 (ArC), 129.21 (2 x ArC), 126.87 (2 x ArC), 93.22 (C-1), 73.43 (C-2), 73.01 (C-3), 72.98 (C-5), 68.56 (C-4), 62.25 (C-6), 20.22 (CH_3CO), 20.18 (CH_3CO), 20.14 (CH_3CO), 20.01 (CH_3CO).

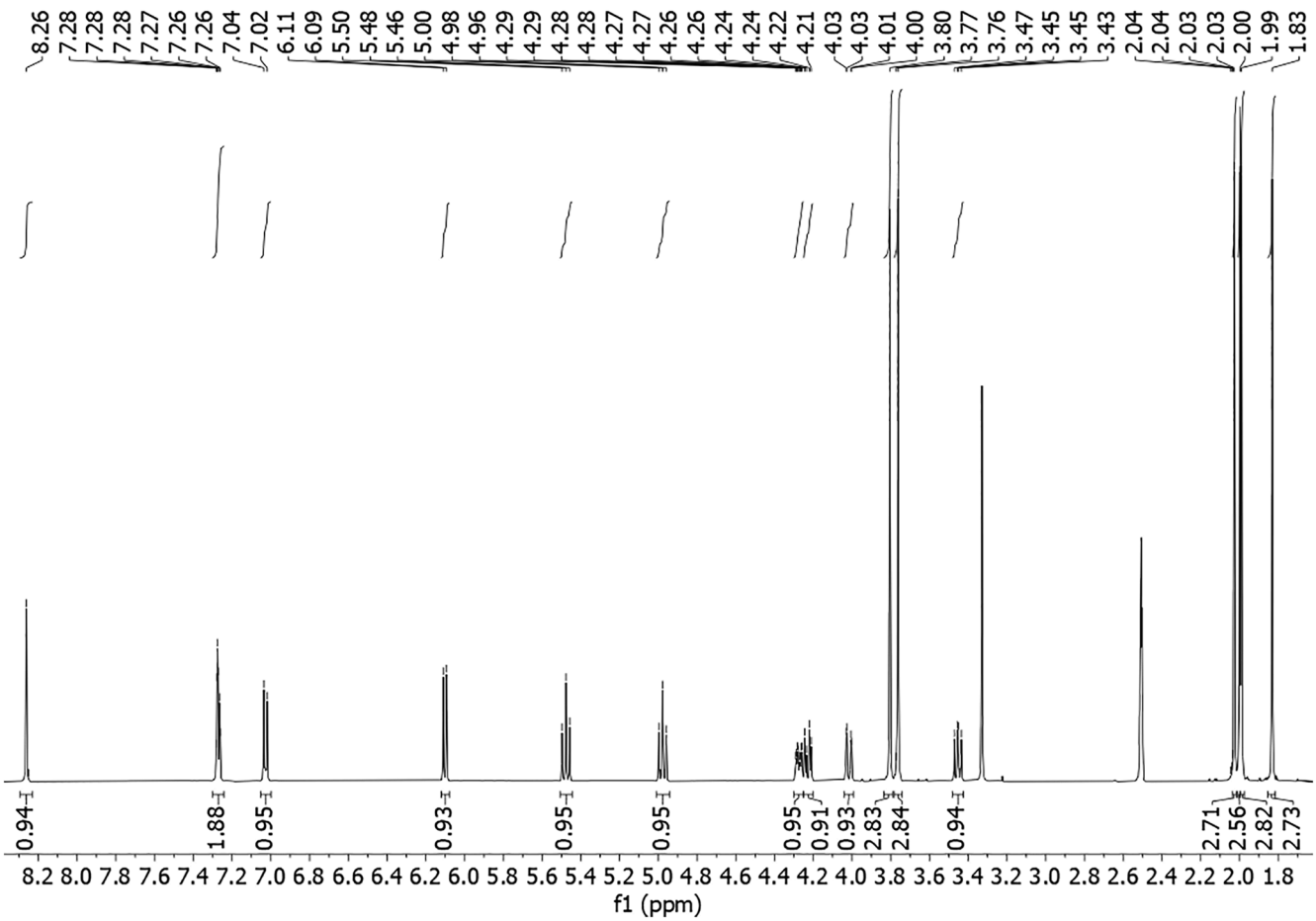

Fig. 2. ^{1}H NMR of glucoimine **5ii**.

Table 2
Experimental and calculated coupling constants of compound **5ii**.

	5ii	Calculated[a],[31]
$J_{H1,H2}$	8.3	7.1
$J_{H2,H3}$	9.7	9.1
$J_{H3,H4}$	9.7	7.2
$J_{H4,H5}$	9.7	8.5
$J_{H5,H6S}$	4.6	8.4
$J_{H5,H6R}$	2.1	1.6

[a] Calculated from the torsion angles of **5ii** in the crystalline form.

2.2. X-ray diffraction analysis

The X-ray diffraction (XRD) structure of compound **5ii** was solved. The measurements were performed on a Rigaku-Oxford, Gemini, Eos CCD diffractometer with graphite-monochromated CuKα (λ = 1.54184 Å) radiation. X-ray diffraction intensities were collected (ω scans with ϑ and κ-offsets), integrated, and scaled with CrysAlisPro [15] suite of programs. The unit cell parameters were obtained by least-squares refinement (based on the angular setting for all collected reflections with intensities larger than seven times the standard deviation of measurement errors) using CrysAlisPro. Data were corrected empirically for absorption employing the multi-scan method implemented in CrysAlisPro. The structure was solved by intrinsic phasing with SHELXT [16] and the molecular model refined with SHELXL [17]. Most H-atoms were found at approximated positions in a difference Fourier map phased on the heavier atoms. However, they were positioned geometrically at their expected locations and refined with the riding model. The methyl H-atoms were treated as rigid groups allowed to rotate during the refinement around the corresponding C—CH_3 bonds such as to maximize the sum of the residual electron density at the hydrogen calculated positions. All -CH_3 groups converged to staggered rotational conformations.

2.3. Inhibition of carbonic anhydrase isozymes

An Applied Photophysics stopped-flow instrument has been used for assaying the CA catalyzed CO_2 hydration activity as reported by Khalifah [18]. Phenol red (at a concentration of 0.02 mM) has been used as indicator, working at the absorbance máximum of 557 nm, with 20 mM Hepes (pH 7.5) as buffer, and 20 mM Na_2SO_4 (for maintaining constant the ionic strength), following the initial rates of the CA-catalyzed CO_2 hydration reaction for a period of 10–100 s. The CO_2 concentrations ranged from 1.7 to 17 mM for the determination of the kinetic parameters and inhibition constants. For each inhibitor, at least six traces of the initial 5–10 % of the reaction have been used for determining the initial velocity. The uncatalyzed rates were determined in the same manner and subtracted from the total observed rates. Stock solutions of inhibitor (0.1 mM) were prepared in distilled–deionized water and dilutions up to 0.01 nM were done thereafter with distilled–deionized water. Inhibitor and enzyme solutions were preincubated together for 15 min at room temperature prior to assay, in order to allow for the formation of the E-I complex. The inhibition constants were obtained by non-linear least-squares methods using PRISM 3, and the Cheng-Prussoff equation [19] as reported earlier, and represent the mean from at least three different determinations.

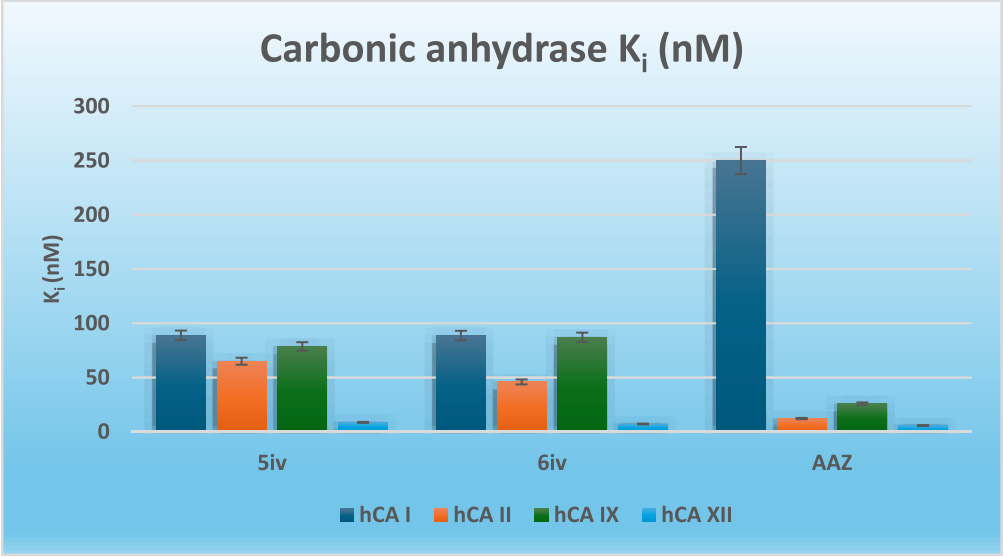

Fig. 3. Carbonic anhydrase inhibition profile of compounds **5iv** and **6iv**.

Table 3
Docking scores with hCAII (PDB 3K34) using $Autodock_{ZN}$ as force field.

Compound	Score
5ii	−7.9
6ii	−5.4
5iv	−10.2
6iv	−9.3

2.4. Computational methodology

The three-dimensional structure of hCAII the target protein (PDB ID: 3K34 [20]) was retrieved from the Protein Data Bank. The protein structure was subjected to essential preprocessing tasks using the Dockprep tool of UCSF Chimera, including the removal of water molecules, addition of hydrogen atoms, and optimization of the hydrogen bonding network. Any co-factors, except Zn^{2+} cation, were also eliminated.

The ligands' structures selected for docking were built with Avogadro molecular editor [21] and optimized with OpenMOPAC 22.1.1 [22], using the semiempirical method PM7. The structures were processed using Meeko [23] to generate pdbqt files. The pdbqt format contains the information required by the protein-ligand docking software AutoDock; in addition to coordinates and atom types of a pdb file, it includes charges and rotatable bonds.

The docking simulations were carried out with AutoDock4 using $AutoDock_{Zn}$ force field [24], a variant for docking studies involving Zn-containing proteins. The grid box was set up with 56, 62, and 64 points in the x, y, and z axis, with a spacing of 0.375 Å, and center in −6.14, 1.87, 17.19 (3K34 cartesian system). AutoGrid 4.2.7, included in the AutoDockFR suite [25], was used to generate grid maps, and Autodock Vina 1.2.5 [26], which is compatible with Autodock4, to run the docking exploration. The exhaustiveness was set to 32, while the other parameters were set to their default values.

Finally, the ligand-protein complexes were subjected to detailed analysis using PoseEdit [27], a software tool for visualizing and analyzing molecular interactions. PoseEdit facilitated the identification and characterization of key interactions, including hydrogen bonds, hydrophobic contacts, and metal-ligand coordination, within the docked complexes.

3. Results and discussion

The deprotected glucoimines **6** were synthesized by condensation d-glucosamine (**1**) with aromatic aldehydes incorporating the methoxy or sulfonamide functionality at room temperature in basic medium as outlined in Scheme 1. The glycoside **6iii** could not be obtained under the conditions described. The per-O-acetylated glucoimines **5** were prepared by a sequence starting with the *N*-[methoxybenzylidene]-d-glucosamine **2**. The imine **2** was acetylated using acetic anhydride in the presence of pyridine to afford the peracetylated derivative **3**. Treatment of glycoside **3** with hydrochloric acid in acetone afforded the acetylated d-glucosamine **4**, which was reacted with the aromatic aldehydes to prepare the acetylated glucoimines **5**. All the imines have been purified by crystallization and/or flash chromatography and fully characterized by ^{1}H and ^{13}H NMR. It is interesting to note that in the NMR spectra of imines **5** and **6** only β-anomers could be detected (see Supplementary information). Crystallization of acetylated glucoimine **5ii** from ethanol afforded single-crystals suitable for X-ray analysis.

Thus, we solved the X-ray diffraction (XRD) structure of the glycoimine **5ii** (Fig. 1 and supplementary material). It crystallizes in the monoclinic space group P21 with two molecules per unit cell. The structures were solved from 2310 reflections with $I > 2\sigma(I)$ and refined to an agreement a R1-factor of 0.0786. The absolute structure, and therefore the chirality of its stereo genic centers, was determined from X-ray anomalous dispersion. To enhance our understanding of the glucoimine's conformation behavior in solution, we also performed the NMR analysis in DMSO.

For glucoimine **5ii**, the pyranose ring adopted a slightly distorted $^{4}C_{1}$ conformation as evidenced by the Cremer Pople parameters (φ=320.380°; θ=12.95°, Q = 0.561) [28]. These parameters are employed to characterize the conformation of rings using spherical polar coordinates obtained from the Fourier transform of the puckering coordinates [29]. Upon close examination of endocyclic torsion angles of the pyranose (Table 1), it is evident that τ(C1–O5–C5–C4), τ(C5–O5–C1–C2), and τ(C3–C4–C5–O5) dihedral angles are around the ideal value for a $^{4}C_{1}$ conformation [30], thus showing that the major distortion in the ring occurs in C-2. It should be explained in terms of the spatial disposition of the imine group. It is noteworthy that in the solid-state structure elucidated for **5ii**, the plane containing the imine functionality is approximately perpendicular to the mean plane of the pyranose ring. This means that the imino group takes on a favored orientation in relation to the pyranose ring, with its lone pair on nitrogen parallel to the axial substituents of the sugar moiety. This orientation

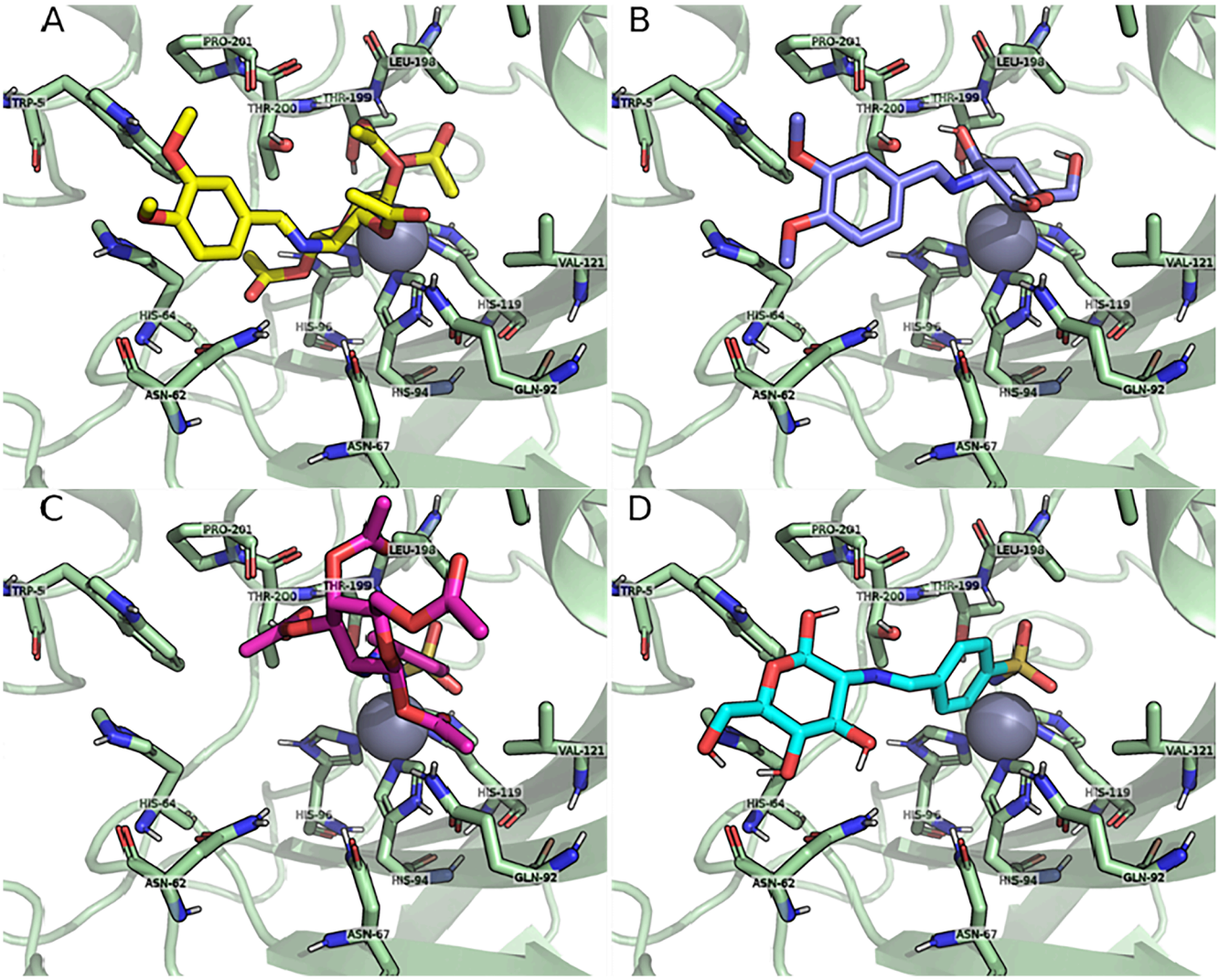

Fig. 4. The best docking pose of the ligands with hCAII (PDB 3K34): A) **5ii**, B) **6ii**, C) **5iv**, D) **6iv**. Zinc cation is represented as a gray sphere, and ligand and neighboring residues are highlighted in stick format. The images were generated using PyMOL [Retrieved from http://www.pymol.org/pymol].

leads to a *syn* arrangement of hydrogen of C-2 and the one of the imine group and as consequence, the H-2 suffers a large deshielding effect (3.45 ppm) as can be seen in the ^{1}H NMR spectra (Fig. 2).

The three bond ^{1}H–^{1}H coupling constants were used to compare the conformations adopted in the solid state and solution (Table 2). The corresponding *J* value was calculated using the Karplus equation modified by Altona [31]. A close examination of *J* values showed that the acetoxymethyl, acetyl, and imine groups are attached by an equatorial linkage to the glucopyranosyl ring, which confirms the $^{4}C_{1}$ conformation of the sugar ring in solution (in DMSO). The differences found could be attributed to molecular distortions by crystal packing forces and the presence of isomers for rotation (rotamers) about the C5-C6 bond in solution. Conformational behavior about the C5–C6 bond in glycosides leads to three staggered orientations namely *gauche-gauche* (*gg*), *trans-gauche* (*tg*), and *gauche-trans* (*gt*). Glucoimine **5ii** shows a preference for the *gt* conformation in the solid state. In solution, the population of rotamers about C5-C6 can be determined using the coupling constants $J_{H5,H6S}$, $J_{H5,H6R,}$ and $J_{H6R\text{-}H6S}$ and the correlations developed by Ohrui [32]. The use of these equations allowed us to estimate that **5ii** exhibits a preference for *gg* rotamer in solution (*gg:gt:tg* 66:31:3). Conformational differences between the solid state and solution can be attributed to the adoption of a more compact molecular structure in the *gt* conformation, resulting in improved crystal packing.

The inhibitory activities of glucoimines **2, 3, 5,** and **6** against cytosolic isoforms hCA I and II, as well as the membrane-associated isoforms hCA IX and XII, were assayed by using stopped flow assay method and acetazolamide as standard inhibitor drug. Only the glucoimines **5iv** and **6iv** incorporating the sulfonamide group showed activity against the CA isozymes (Fig. 3 and supplementary information). These findings were unexpected as our previous research has demonstrated that attaching carbohydrate moieties to CA methoxyaryl or phenol pharmacophores improves and/or enhances its inhibitory activity [11,14].

In designing CA inhibitors, a crucial factor to consider is the specificity for inhibiting the tumor-related isoforms (hCA IX and XII) in comparison to the commonly found cytosolic forms (hCA I and II). Glycosides **5iv** and **6iv** showed very good inhibition against cancer-related isozymes, however, no selectivity was found in the inhibition of hCA IX and hCA II (Fig. 3). The physicochemical properties of our glucoimines could overcome this lack of selectivity. The design of inhibitors that do not permeate the cell membrane is essential in developing anti-cancer compounds that selectively target the membrane-bound isoforms hCA IX and hCA XII, as opposed to the widely distributed isoform CA II. The calculated *m*Log*P* parameter usually shows a strong correlation with experimental permeability data [33]. Molecules with *m*Log*P* values ranging from 1 to 3 generally exhibit good passive membrane permeability, while those with *m*Log*P* values below 0 are

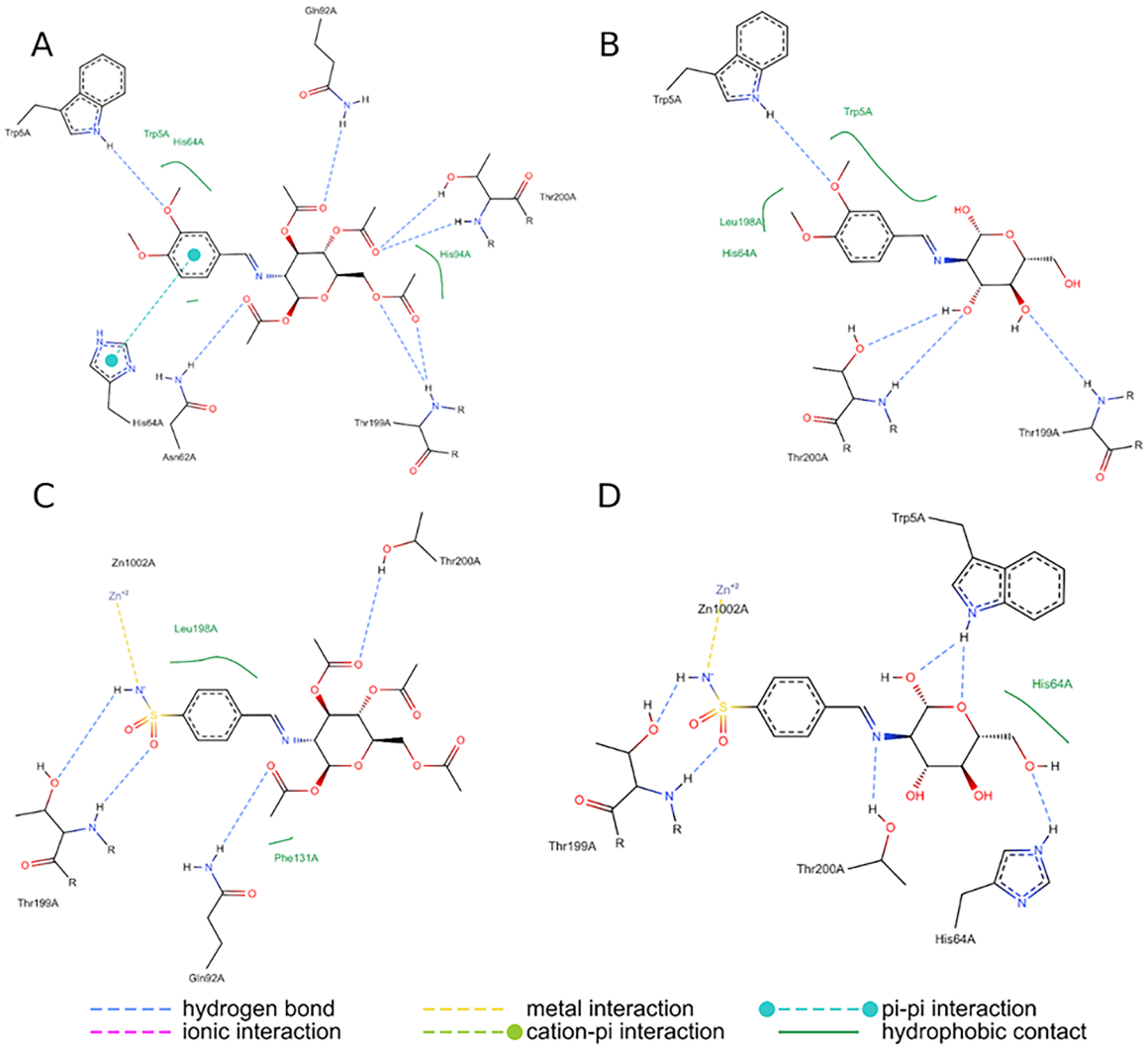

Fig. 5. 2D ligand interaction diagrams for selected ligands with hCAII (PDB 3K34): (A) **5ii**, (B) **6ii**, (C) **5iv**, (D) **6iv**. Analyses were done using PoseEdit [27].

more likely to have limited ability to penetrate cell membranes. Calculated mLogP value of −1.45 [34] for the glucoimine and **6iv** show that the poor passive membrane permeability of the deprotected imine would favor the preferential inhibition of CAs IX and XII over ubiquitous cytosolic hCA II. It should be noted that compound per-O-acetylated glucoimine **5iv** may be used as ester prodrug for oral delivery. Once in the body, the acetate groups of **5iv** could be readily hydrolyzed by ubiquitous esterases resulting in the formation of the compound **6iv**, which will reach the tumor cell.

Docking simulations were performed for selected compounds veratrole glucoimines **5ii** and **6ii** and sulfonamide glucoimines **5iv** and **6iv** with hCAII using AutoDock$_{Zn}$ scripts and force field, which was calibrated on a data set of 292 crystal complexes containing zinc [24].

The obtained scores are summarized in Table 3. Remarkably, there is a correlation between the docking scores (more negative, more favorable) and the experimental inhibition activity against hCAII presented by the compounds.

The 3D structure of ligand-hCAII complexes shown in Fig. 4, complexes and interaction analyses (Fig. 5) revealed a main difference between **5ii** and **6ii**, with respect to **5iv** and **6iv**: the latter showing an interaction of the sulfonamide group with Zn^{2+}cation. The position of the sulfonamide group in the active site is similar to that found in other CAIs possessing the same pharmacophore. This difference also causes the carbohydrate moiety to be oriented towards the outside of the active site in the case of **5iv** and **6iv**, exposed to the solvent, while in **5ii** and **6ii** they were oriented towards the inside of the pocket.

On the other hand, it should be noted that all four ligands showed hydrogen bonding interactions with Thr199 and Thr200, residues in the deep part of the catalytic pocket.

4. Conclusion

In conclusion, a series of glucoimines has been prepared by condensation of d-glucosamine and aromatic aldehydes incorporating classical and non-classical CA pharmacophores. It was possible to study the conformational behavior in solution and in the crystalline form of veratrole derivative **5ii** by NMR and X-ray diffraction analysis showing that the sugar ring has essentially the same $^4C_1$ conformation. All glucoimines were tested against four isozymes of carbonic anhydrase comprising hCAs I and II (cytosolic, ubiquitous isozymes) and hCAs IX and XII (tumor-associated isozymes). In this study, per-O-acetylated glucoimine **5iv** and deprotected compound **6iv**, both incorporating the sulfonamide moiety, were identified as potent inhibitors of carbonic anhydrase isozymes. Molecular docking simulation was performed inside the active site of hCA II to evaluate the binding modes of selected compounds. Promising compounds **5iv** and **6iv** demonstrated the most favorable docking scores, indicating strong binding affinity towards hCAII and in correlation with experimental inhibition activities. Interestingly, the interaction analyses of ligand-hCAII complexes showed distinct binding modes between **5ii**/**6ii** and **5iv**/**6iv**, primarily due to

the sulfonamide group.

CRediT authorship contribution statement

Ivana R. Vásquez: Investigation. **Leonardo E. Riafrecha:** Investigation. **Leandro Martínez Heredia:** Investigation. **Gustavo A. Echeverría:** Investigation. **Oscar E. Piro:** Investigation. **Martín J. Lavecchia:** Methodology, Investigation. **Claudiu T. Supuran:** Investigation. **Pedro A. Colinas:** Writing – original draft, Methodology, Investigation, Conceptualization.

Declaration of competing interest

There are no conflicts to declare.

Data availability

Data will be made available on request.

Acknowledgment

This work was financed by UNLP (11X/927 and 11/X958), CONICET (PIP1695 and PIP0651) and ANPCYT (PICT 2019–02578, PICT 2021-I-A-00412). I.R.V. and L. M. H. are holders of fellowships from CONICET. G.A.E., O.E.P, L. E. R., M. J. L., and P.A.C. are members of the Scientific Research Career of CONICET. Thanks are also due to Lic. Omar Guaymas for valuable help on NMR measurements. Crystallographic structural data have been deposited at the Cambridge Crystallographic Data Centre (CCDC) with reference numbers CCDC 2339800. These data can be obtained free of charge from The Cambridge Crystallographic Data Centre via www.cc dc.cam.ac.uk/data_request/cif.

Supplementary materials

Supplementary material associated with this article can be found, in the online version, at doi:10.1016/j.molstruc.2024.139778.

References

[1] D. Iacopetta, J. Ceramella, A. Catalano, C. Saturnino, M.G. Bonomo, C. Franchini, M.S. Sinicropi, Schiff bases: interesting scaffolds with promising antitumoral properties, Appl. Sci. 11 (4) (2021) 1877, https://doi.org/10.3390/app11041877.
[2] Y. Jia, J.B. Li, Molecular assembly of Schiff base interactions: construction and application, Chem. Rev. 115 (3) (2015) 1597–1621, https://doi.org/10.1021/cr400559g.
[3] M. Bergmann, L. Zervas, Synthesen mit glucosamine, Ber. O Chem. Ber. *(A and B Series)* 64 (5) (1931) 975–980, https://doi.org/10.1002/cber.19310640506.
[4] H. Kunz, Selectivities in Lewis acid promoted reactions, in: D. Schinzer, Kluwer Academic: Dordrecht, London, 1989, pp 189–202.
[5] J. Costamagna, L.E. Lillo, B. Matsuhiro, M.D. Noseda, M. Villagrán, Ni (II) complexes with Schiff bases derived from amino sugars, Carbohydr. Res. 338 (15) (2003) 1535–1542, https://doi.org/10.1016/S0008-6215(03)00237-4.
[6] A. Kumar, N.K. Singhal, B. Ramanujam, A. Mitra, N.R. Rameshwaram, S. K. Nadimpalli, C.P. Rao, C 1-/C 2-aromatic-imino-glyco-conjugates: experimental and computational studies of binding, inhibition and docking aspects towards glycosidases isolated from soybean and jack bean, Glycoconj. J. 26 (2009) 495–510, https://doi.org/10.1007/s10719-008-9199-4.
[7] A. Kumar, A. Mitra, A.K. Ajay, M.K. Bhat, C.P. Rao, Cu (II) complexes of glyco-imino-aromatic conjugates in DNA binding, plasmid cleavage and cell cytotoxicity, J. Chem. Sci 124 (2012) 1217–1228, https://doi.org/10.1007/s12039-012-0319-0.
[8] S. Tabassum, S. Yadav, F. Arjmand, Synthesis and mechanistic insight of glycosylated CuII/NiII–Sn2IV heterobimetallic DNA binding agents: validation of a specific CuII–Sn2IV chemotherapeutic agent for human leukemic cell line K-562, J. Organomet. Chem 745 (2013) 226–234, https://doi.org/10.1016/j.jorganchem.2013.07.077.
[9] P. Mokhtari, G. Mohammadnezhad, Anti-cancer properties and catalytic oxidation of sulfides based on vanadium (V) complexes of unprotected sugar-based Schiff-base ligands, Polyhedron 215 (2022) 115655, https://doi.org/10.1016/j.poly.2022.115655.
[10] J.Y. Winum, P.A. Colinas, C.T. Supuran, Glycosidic carbonic anhydrase IX inhibitors: a sweet approach against cancer, Bioorg. Med.Chem. 21 (2013) 1419–1426, https://doi.org/10.1016/j.bmc.2012.10.043.
[11] H.L. Martínez, L.E. Riafrecha, P.A. Colinas, C-cinnamoyl glycosides: an emerging "Tail" for the development of selective carbonic anhydrase inhibitors, Curr. Med. Chem. 26 (15) (2019) 2601–2608, https://doi.org/10.2174/0929867325666180713122907.
[12] J.K. Kim, C. Lee, S.W. Lim, A. Adhikari, J.T. Andring, R. McKenna, C.M. Ghim, C. U. Kim, Elucidating the role of metal ions in carbonic anhydrase catalysis, Nat. Commun. 11 (1) (2020) 4557, https://doi.org/10.1038/s41467-020-18425-5.
[13] S.G. Nerella, P.S. Thacker, M. Arifuddin, C.T. Supuran, Tumor-associated carbonic anhydrase inhibitors: rational approaches, design strategies, structure-activity relationship and mechanistic insights, Eur. J. Med. Chem. Rep. 10 (2024) 100131, https://doi.org/10.1016/j.ejmcr.2024.100131.
[14] M.S. Le Pors, L. Santa Maria de la Parra, L.E. Riafrecha, D. Vullo, I.E. León, C. T. Supuran, P.A. Colinas, Glycosyl isoxazoles for targeting of tumor microenvironment and cancer cells: highly selective inhibitors of carbonic anhydrases IX and XII showing cytotoxic activity, ChemistrySelect 8 (11) (2023) e202300039, https://doi.org/10.1002/slct.202300039.
[15] O.D. Rigaku, CrysAlis PRO (version 1.171.38.41) Yarnton, England, 2015.
[16] G.M. Sheldrick, SHELXT - Integrated space-group and crystal-structure determination, Acta Cryst. A71 (2015) 3–8.
[17] G.M. Sheldrick, A short history of SHELX, Acta Cryst A64 (2008) 112–122.
[18] R.G. Khalifah, The carbon dioxide hydration activity of carbonic anhydrase: I. Stop-flow kinetic studies on the native human isoenzymes B and C, J. Bio. Chem. 246 (8) (1971) 2561–2573, https://doi.org/10.1016/S0021-9258(18)62326-9.
[19] C. Yung-Chi, W.H. Prusoff, Relationship between the inhibition constant (K_I) and the concentration of inhibitor which causes 50 per cent inhibition (I_{50}) of an enzymatic reaction, Biochem. Pharmacol. 22 (23) (1973) 3099–3108, https://doi.org/10.1016/0006-2952(73)90196-2.
[20] C.A. Behnke, I. Le Trong, J.W. Godden, E.A. Merritt, D.C. Teller, J. Bajorath, R. E. Stenkamp, Atomic resolution studies of carbonic anhydrase II, Acta Crystallogr. D Biol. Crystallogr. 66 (5) (2010) 616–627, https://doi.org/10.1107/S0907444910006554.
[21] M.D. Hanwell, D.E. Curtis, D.C. Lonie, T. Vandermeersch, E. Zurek, G.R. Hutchison, Avogadro: an advanced semantic chemical editor, visualization, and analysis platform, J. Cheminform. 4 (2012) 1–17, https://doi.org/10.1186/1758-2946-4-17.
[22] Molecular Sciences Software Institute (MolSSI), Molecular Orbital PACkage (MOPAC). https://github.com/openmopac/mopac, 2021 (2024).
[23] Forli lab at the Center for Computational Structural Biology (CCSB), Meeko: preparation of small molecules for AutoDock. https://github.com/forlilab/Meeko, 2024 (accessed 30 March 2024).
[24] D. Santos-Martins, S. Forli, M.J. Ramos, J A, Olson AutoDock4Zn: an improved AutoDock force field for small-molecule docking to zinc metalloproteins, J. Chem. Inf. Model. 54 (8) (2014) 2371–2379, https://doi.org/10.1021/ci500209e.
[25] P.A. Ravindranath, S. Forli, D.S. Goodsell, A.J. Olson, M.F. Sanner, AutoDockFR: advances in protein-ligand docking with explicitly specified binding site flexibility, PLoS Comput. Biol. 11 (12) (2015) e1004586, https://doi.org/10.1371/journal.pcbi.1004586.
[26] J. Eberhardt, D. Santos-Martins, A.F. Tillack, S. Forli, AutoDock Vina 1.2. 0: new docking methods, expanded force field, and python bindings, J. Chem. Inf. Model. 61 (8) (2021) 3891–3898, https://doi.org/10.1021/acs.jcim.1c00203.
[27] K. Diedrich, B. Krause, O. Berg, M.PoseEdit Rarey, Enhanced ligand binding mode communication by interactive 2D diagrams, J. Comput. Aided Mol. Des. 37 (10) (2023) 491–503, https://doi.org/10.1007/s10822-023-00522-4.
[28] http://enzyme13.bt.a.u-tokyo.ac.jp/CP/, 2024 (17 May 2024).
[29] D.T. Cremer, J. Pople, A General definition of ring puckering coordinates, J. Am. Chem. Soc. 97 (6) (1975) 1354–1358, https://doi.org/10.1021/ja00839a011.
[30] A. Bérces, D.M. Whitfield, T. Nukada, Quantitative description of six-membered ring conformations following the IUPAC conformational nomenclature, Tetrahedron 57 (3) (2001) 477–491, https://doi.org/10.1016/S0040-4020(00)01019-X.
[31] C.A.G. Haasnoot, F.A. de Leeuw, C. Altona, The relationship between proton-proton NMR coupling constants and substituent electronegativities—I: an empirical generalization of the Karplus equation, Tetrahedron 36 (19) (1980) 2783–2792, https://doi.org/10.1016/0040-4020(80)80155-4.
[32] Y. Nishida, H. Hori, H. Ohrui, H. Meguro, ^{1}H NMR analyses of rotameric distribution of C5-C6 bonds of D-glucopyranoses in solution, J. Carbohydr. Chem. 7 (1) (1988) 239–250, https://doi.org/10.1080/07328308808058917.
[33] E.H. Kerns, L. Di, Drug-like Properties: Concepts, Structure Design and Methods: From ADME to Toxicity Optimization, London, 2008.
[34] Swiss Institute of Bioinformatics, Swiss Adme. http://swissadme.ch/index.php, 2017 (accessed 17 May 2024).